Analysis of vortex induced vibration of a thermowell by high fidelity FSI numerical analysis based on RBF structural modes embedding

Alessandro Felici[1], Antonio Martínez-Pascual[1], Corrado Groth[1], Leonardo Geronzi[1], Stefano Porziani[1], Ubaldo Cella[1], Carlo Brutti[1], and Marco Evangelos Biancolini[1][0000-0003-0865-5418]

[1] Department of Enterprise Engineering, University of Rome Tor Vergata, Roma, Italy
biancolini@ing.uniroma2.it

Abstract. The present paper addresses the numerical fluid-structure interaction (FSI) analysis of a thermowell immersed in a water flow. The study was carried out implementing a modal superposition approach into a computational fluid dynamics (CFD) solver. The core of the procedure consists in embedding the structural natural modes, computed by a finite element analysis (FEA), by means of a mesh morphing tool based on radial basis functions (RBF). In order to minimize the distortion during the morphing action and to obtain a high quality of the mesh, a set of corrective solutions, that allowed the achievement of a sliding morphing on the duct surface, was introduced. The obtained numerical results were compared with experimental data, providing a satisfying agreement and demonstrating that the modal approach, with an adequate mesh morphing setup, is able to tackle unsteady FSI problems with the accuracy needed for industrial applications.

Keywords: Morphing, Radial Basis Functions, Multi-physics, RBF, FSI, Fluid-Structure Interaction, Vortex-Induced Vibration, Modal superposition, Sliding morphing, Thermowell

1 Introduction

Today the need of developing multi-physics approaches to address complex design challenges is rising. The numerical methods adopted must involve coupled-field analyses that allow evaluating the combined effects of the multiple physical phenomena acting on a given system. One of the most interesting and with a wide range of application multi-physics phenomenon is the interaction between a fluid and a structure. This interaction can occur for several reasons: it can be the working principle of the system; it can be aimed to the lightweight design of the structure or it can be exploited to finely tune the design.

The fluid structure interaction (FSI) mechanism plays a fundamental role in a wide range of engineering fields, such as automotive, aerospace, marine, civil and biomedical. The numerical approaches adopted to couple the computational fluid dynamics

ICCS Camera Ready Version 2021
To cite this paper please use the final published version:
DOI: 10.1007/978-3-030-77977-1_37

(CFD) and computational structural mechanics (CSM) codes can be classified according to two main categories: the monolithic approach and the partitioned approach. In the former the fluid dynamics and the structural dynamics models are solved simultaneously within a unified solver; in the latter they are solved separately, with two distinct solvers. Whatever type of approach is chosen, the deformation of the CFD mesh is needed in order to accommodate the shape changes of the structure. In the present work a mesh morphing algorithm based on radial basis functions (RBF) will be used to update the CFD mesh according to the deformed shape of the structure. The FSI approach here proposed allows to adapt the mesh to the shape of the deformable structure by a superposition of its natural modes during the progress of the CFD computation. This method proved in the past its efficiency and reliability in many studies for both steady [1, 2] and unsteady flows [3, 4]. Its main limit is that it cannot be directly employed in problems involving non-linearities of any kind, contact or pre-stressed components.

The underlying idea of the proposed workflow is that at each time-step the fluid forces over the structure surface, together with inertial loads, are computed as modal forces to determine the amplitude of each modal shape. Superimposing the modal shapes, the overall deformation of the structure is deducible at each instant and can be imposed by mesh morphing. The method is implemented to investigate an industrial problem: the vortex induced vibration of a thermowell immersed in a fluid flow.

Thermowells are cylindrical fittings used to protect temperature sensors (as for example thermometers or thermocouples) installed in industrial processes. In such setup the fluid transfers heat to the thermowell wall which, in turn, transfers heat to the sensor. The usage of a thermowell, other than protecting the sensor from the pressure and chemical effects of the process fluid, allows to easily replace the sensor without draining the vessel or the piping. Thermowells, however, are subjected to the risk of flow-induced vibrations generated by vortex shedding which might lead to bending fatigue failure. Hence, in modern applications involving high strength piping and elevated fluid velocity, the dynamics of the system have to be carefully evaluated to foresee ad-hoc countermeasure to limit this phenomenon, such as for example twisted square thermowells. A numerical method able to reliably reproduce the fluid and structural coupling is therefore needed to quickly evaluate different designs and reduce the time to market of new products.

In the present work, authors will first give an introduction of the proposed FSI approach, then its application to an industrial problem will be illustrated and finally the study results will be detailed and discussed.

2 Theoretical background

2.1 Unsteady FSI using modal superposition

The FSI approach used in this work is based on the modal theory [3, 5]: the structural deformation can be thought as a linear superimposition of the modal shapes of the body itself, so that by importing the modal shapes in the CFD solver with a mesh morphing tool, the fluid dynamic numerical configuration can be made implicitly aeroelastic.

ICCS Camera Ready Version 2021
To cite this paper please use the final published version:
DOI: 10.1007/978-3-030-77977-1_37

For a generic n-degrees-of-freedom system (for example n masses virtually positioned on the nodes of the mesh for a FEM structural analysis), the second order differential system of equations of motion can be written in matrix form as (1) [6]:

$$[\boldsymbol{M}]\ddot{\boldsymbol{y}} + [\boldsymbol{C}]\dot{\boldsymbol{y}} + [\boldsymbol{K}]\boldsymbol{y} = \boldsymbol{Q} \tag{1}$$

Where: $[\boldsymbol{M}]$ is the mass matrix, $[\boldsymbol{C}]$ is the damping matrix, $[\boldsymbol{K}]$ is the stiffness matrix, $\boldsymbol{Q}$ is the external forces vector (that may vary in time), $\boldsymbol{y}$ is the generalized coordinates vector. Being the modal shapes linearly independent, a new reference system in which the equations can be uncoupled is introduced so that each contribution of a mode to the total structure deformation is isolated:

$$\boldsymbol{q} = [\boldsymbol{v}]^{-1}\boldsymbol{y} \tag{2}$$

Where: $\boldsymbol{q}$ is the vector of modal coordinates and $[\boldsymbol{v}]$ is the modal matrix, whose columns are the mass-normalized natural modes. By substituting this definition in equation (1), pre-multiplying by $[\boldsymbol{v}]^{\mathrm{T}}$ both terms and retaining the mass normalization of the modal shapes, the following equation is obtained:

$$[\boldsymbol{I}]\ddot{\boldsymbol{q}} + [\boldsymbol{v}]^T[\boldsymbol{C}][\boldsymbol{v}]\dot{\boldsymbol{q}} + [\boldsymbol{v}]^T[\boldsymbol{K}][\boldsymbol{v}]\boldsymbol{q} = [\boldsymbol{v}]^T\boldsymbol{Q} \tag{3}$$

The term on the right-hand side of the equation is referred to as modal force vector, computed integrating the projection of the nodal forces on the surfaces onto the relevant mode. The solution to this equation, describing the temporal evolution of each modal coordinate, can be deduced by recurring to the Duhamel's integral:

$$\begin{aligned} q(t) = e^{-\varsigma\omega_n t}\left[q_0\cos(\omega_d t) + \frac{\dot{q_0}+\varsigma\omega_n q_0}{\omega_d}\sin(\omega_d t)\right] + \\ +e^{-\varsigma\omega_n t}\left\{\frac{1}{m\omega_d}\int_0^t e^{-\frac{b(t-\tau)}{2m}} f(\tau)\sin[\omega_d(t-\tau)]d\tau\right\} \end{aligned} \tag{4}$$

Where: ω_n is the natural circular frequency of the considered mode, ς is the damping factor, ω_d is the damped circular frequency, q_0 and $\dot{q_0}$ are the boundary conditions (respectively initial modal coordinates and initial modal velocities), m is the modal mass (unitary if the mass normalization is implemented).

2.2 RBF Mesh morphing

RBF are mathematical functions able to interpolate, on a distance basis, the scalar information known at defined source points of a domain in which the functions are not zero valued. They can be defined in an n-dimensions space and are function of the Euclidean norm of the distance between two points in the space. The interpolation function is composed of a radial function ϕ and a polynomial term h, whose degree depends on the chosen basis. This polynomial term is added to assure uniqueness of the problem and polynomial precision, allowing to prescribe rigid body translations. If m is the number of source points, the interpolation function can be written as follows:

$$s(\boldsymbol{x}) = \sum_{i=1}^{m}\gamma_i\phi\left(\left\|\boldsymbol{x} - \boldsymbol{x}_{k_i}\right\|\right) + h(\boldsymbol{x}) \tag{5}$$

ICCS Camera Ready Version 2021
To cite this paper please use the final published version:
DOI: 10.1007/978-3-030-77977-1_37

Where $\boldsymbol{x}_{k_i}$ is the position vector of the i-th source point.

A radial basis interpolation exists if the coefficients γ and the weights of the polynomial term allow to guarantee the exact function values at the source points and the polynomial term satisfies the orthogonality conditions. Mathematically:

$$s(\boldsymbol{x}_{k_i}) = g_i, 1 \leq i \leq m \tag{6}$$

$$\sum_{i=1}^{m} \gamma_i P(\boldsymbol{x}_{k_i}) = 0 \tag{7}$$

Where: g_i is the known value of the function at the i-th source point; (7) has to be written for all polynomials P with a degree less than or equal to that of polynomial h [7]. The minimal degree of polynomial h depends on the chosen RBF.

A unique interpolation solution exists if the basis function is a conditionally positive definite function [8]. If the basis functions are conditionally positive definite of order less than or equal to two [9], a linear polynomial h can be used:

$$h(\boldsymbol{x}) = \beta_1 + \beta_2 x_1 + \beta_3 x_2 + \cdots + \beta_{n+1} x_n \tag{8}$$

The values for the coefficients γ of the RBF and the weights β of the linear polynomial h can be obtained by solving the system:

$$\begin{bmatrix} \boldsymbol{A} & \boldsymbol{P} \\ \boldsymbol{P}^T & \boldsymbol{0} \end{bmatrix} \begin{pmatrix} \boldsymbol{\gamma} \\ \boldsymbol{\beta} \end{pmatrix} = \begin{pmatrix} \boldsymbol{g} \\ \boldsymbol{0} \end{pmatrix} \tag{9}$$

Where $[\boldsymbol{A}]$ is the interpolation matrix obtained by calculating all the radial interactions among source points, with the radial distances between them:

$$A_{ij} = \phi\left(\left\|\boldsymbol{x}_{k_i} - \boldsymbol{x}_{k_j}\right\|\right), 1 \leq i \leq m\,, 1 \leq j \leq m \tag{10}$$

$[\boldsymbol{P}]$ is the constraint matrix that results from balancing the polynomial contribution. If the space in which the RBF is defined is the physical one, it contains the coordinates of the source points in the space:

$$[\boldsymbol{P}] = \begin{bmatrix} 1 & x_{k_1} & y_{k_1} & z_{k_1} \\ 1 & x_{k_2} & y_{k_2} & z_{k_2} \\ \vdots & \vdots & \vdots & \vdots \\ 1 & x_{k_m} & y_{k_m} & z_{k_m} \end{bmatrix} \tag{11}$$

It is clear that the RBF interpolation works for scalar fields. For the smoothing problem (in which, formally, a vector field is prescribed) each component of the displacement filed prescribed at the source points is interpolated, once the weights and the coefficients of the system have been obtained solving the system 9 for each component (i.e. the three directions in space x, y and z), as follows:

$$\begin{cases} s_x(\boldsymbol{x}) = \sum_{i=1}^{m} \gamma_i^x \phi\left(\left\|\boldsymbol{x} - \boldsymbol{x}_{k_i}\right\|\right) + \beta_1^x + \beta_2^x x + \beta_3^x y + \beta_4^x z \\ s_y(\boldsymbol{x}) = \sum_{i=1}^{m} \gamma_i^y \phi\left(\left\|\boldsymbol{x} - \boldsymbol{x}_{k_i}\right\|\right) + \beta_1^y + \beta_2^y x + \beta_3^y y + \beta_4^y z \\ s_z(\boldsymbol{x}) = \sum_{i=1}^{m} \gamma_i^z \phi\left(\left\|\boldsymbol{x} - \boldsymbol{x}_{k_i}\right\|\right) + \beta_1^z + \beta_2^z x + \beta_3^z y + \beta_4^z z \end{cases} \tag{12}$$

ICCS Camera Ready Version 2021
To cite this paper please use the final published version:
DOI: 10.1007/978-3-030-77977-1_37

The meshless nature of the morphing method appears clear, because the final configuration of the controlled nodes only depends on their original position. Therefore, grid points are moved regardless of element type or connection. This allows the implementation of the RBF to prescribe deformations to the surface mesh and for volume mesh smoothing. In literature RBF were successfully employed in a broad spectrum of applications, from optimizations based on zero order [10] or higher order methods [11, 12, 13], evolutionary optimization mimicking nature [14], load transfer [15], but also for ice accretion [16], fracture mechanics studies [17, 18, 19] and structural results post-processing [20, 21, 22].

The morphing approach allows to apply shape modifications directly to the numerical domain avoiding a remeshing procedure, saving time and preserving computational consistency. When thinking about the number of shape modifications that occur during an unsteady FSI analysis, the advantages of the mesh morphing approach are evident.

2.3 Modal FSI implementation

Starting from the undeformed configuration, the flexible components of the system are modelled and studied by means of a structural modal analysis in order to extract a selected number of eigenvectors. The obtained modes are used to generate an RBF solution for each shape. In this step the far field conditions and the rigid surfaces need to be constrained, whereas the FEM results need to be mapped on the deformable surfaces of the CFD domain. The RBF solutions obtained constitute the modal base that, opportunely amplified, allows to represent the structural deformation under load generating an intrinsically aeroelastic domain. This process is known as “RBF structural modes embedding”. To speed up the mesh morphing step, the deformations associated with each modal shape are stored in memory allowing a morphing action cost that is in the order of a single CFD iteration.

The proposed FSI modelling technique falls into the class of weak approaches because, for an unsteady analysis, loads are considered frozen during each time-step. The modal forces are computed on the prescribed surfaces (i.e. the deformable ones) by projecting the nodal forces (pressure and shear stresses) onto the modal shapes. The mesh is updated during the progress of the CFD computation every prescribed number of iterations, according to the computed modal coordinates. The mesh morphing tool used is RBF Morph™ [23]. CFD and FEM solvers adopted are Ansys Fluent and Ansys Mechanical 2020 R1.

3 Experimental investigation

The investigated industrial problem concerns the vortex induced vibration of a thermowell immersed in a fluid flow. The case study was experimentally measured and recorded by Emerson Electric Co. [24], the multinational corporation that owns the manufacturer of the studied thermowell. The aim of the experiment was to evaluate the flow induced vibrations of the traditional cylindrical thermowell design. The sensor, 470.219 mm in length, was equipped with an accelerometer in the tip and immersed in

ICCS Camera Ready Version 2021
To cite this paper please use the final published version:
DOI: 10.1007/978-3-030-77977-1_37

a water flow inside a 152.4 mm diameter pipe. The water velocity ranged from 0 m/s to 8.5 m/s. The accelerometer allowed the reconstruction of the evolution of the tip displacement. The gathered results are summarized in Fig. 1, in terms of the root mean square of the tip displacement as a function of the fluid velocity.

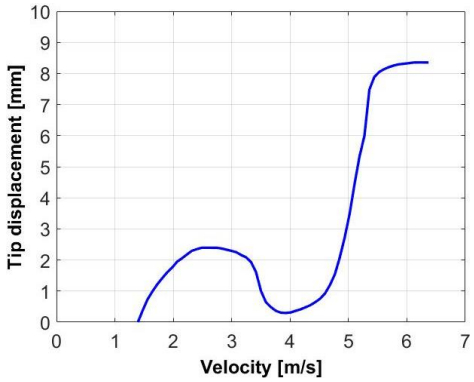

Fig. 1. Experimental results, RMS tip displacement vs fluid velocity

The presence of two lock-in regions is observed: an in-line vibration lock-in and a transverse vibration lock-in region. In the in-line vibration lock-in region the maximum root mean square tip displacement in the streamwise direction is 2.33 mm, registered with a 2.44 m/s fluid velocity. In the transverse vibration lock-in region the maximum root mean square tip displacement in the cross-flow direction is 8.3 mm, registered with a 6.4 m/s fluid velocity. The vibration is induced by organized vortices that shed in sheets along the axial length of the stem and involve the generation of alternating forces. If the shedding frequency approaches a natural frequency of the thermowell or its half (generating the transverse or the in-line vibrations respectively) a failure of the sensor might occur. The failure conditions were reached for the cylindrical thermowell at velocity larger than 6.4 m/s.

The aim of this work was to numerically capture the transverse vibration lock-in region of the cylindrical thermowell.

4 Numerical analysis

4.1 Modal analysis

Fig. 2 reports the configuration of the numerical domain. It consists of a pipe with a diameter of 152.4 mm having a 50.8 mm aperture which houses a 470.219 mm long cylindrical thermowell whose diameter is 16.764 mm. The exposed length of the thermowell is about 143 mm.

ICCS Camera Ready Version 2021
To cite this paper please use the final published version:
DOI: 10.1007/978-3-030-77977-1_37

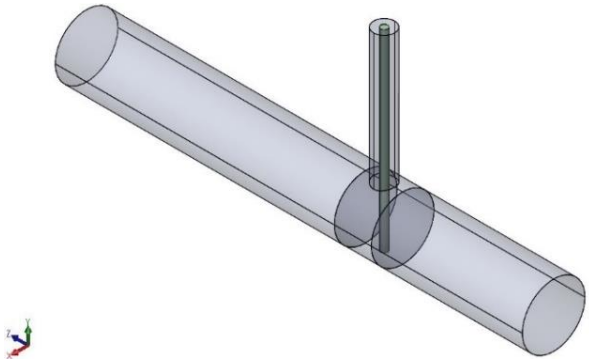

Fig. 2. CAD model of the analyzed system

The thermowell is made of a 304/304L dual rated steel with a density of 7750 kg/m^3, a Young's modulus of 200 GPa and a Poisson's ratio of 0.3 [25]. It was discretized by a uniform mesh made of 34456 20-noded hexahedrons for a total of 148675 nodes. The sensor was modelled as a cantilever beam. The first six modes were extracted from the FEM modal analysis and adopted to populate the modal base adopted for the FSI analysis. The shapes of the six modes are reported in Fig. 3.

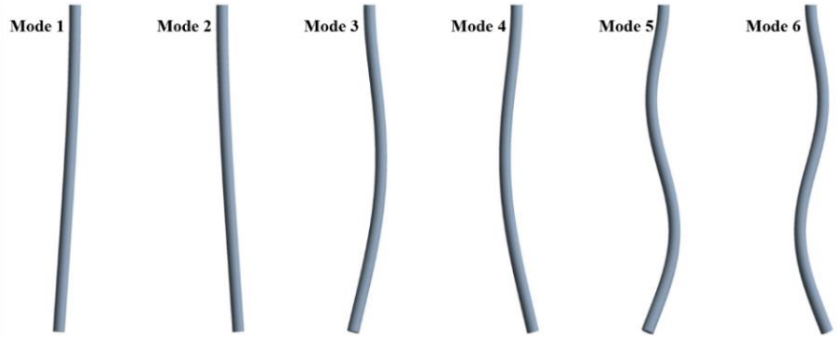

Fig. 3. First six modal shapes

4.2 RBF solutions setup

The shapes of the modes were extracted in terms of displacements of the mesh nodes belonging to the surface of the sensor normalized with respect to the mass. To generate the RBF solution for each natural mode a so-called *two-step* technique was employed [26]. This procedure provides a smother solution and better quality of the morphed mesh. In the first step an RBF solution is generated applying the nodal displacement corresponding to the selected modal shape to the surface mesh of the sensor only, so that the surfaces are exactly morphed in the desired modified configuration, i.e. the one imposed by modal deformation. In the second step the first RBF solution is imposed as a motion law to the thermowell surface together with additional morphing set-up and the surrounding volume domain is then morphed accordingly.

ICCS Camera Ready Version 2021
To cite this paper please use the final published version:
DOI: 10.1007/978-3-030-77977-1_37

The proximity of the tip of the thermowell to the boundary wall of the pipe caused a challenging problem. In fact the large displacements that the thermowell is expected to experience due to the vortex induced vibrations, combined to the requirement of maintaining a cylindrical shape of the pipe wall, would involve a significant distortion of the mesh if the duct wall nodes were imposed as fixed. The effect of such setup is evident comparing the starting (undeformed) mesh (Fig. 4 on the left) with the mesh resulting from a lateral displacement of the sensor in the region of the thermowell tip (Fig. 4 on the right).

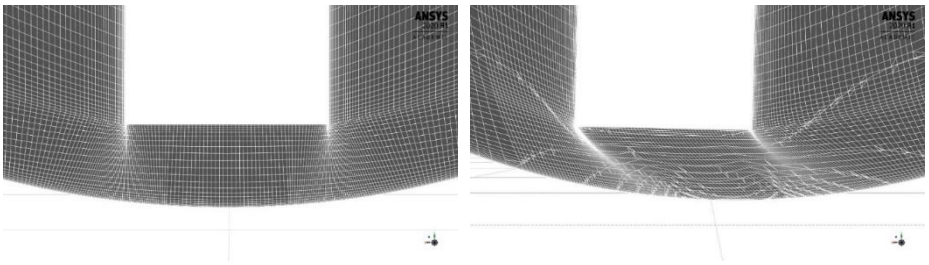

Fig. 4. Starting (left) and deformed (right) mesh around the tip

To avoid the high mesh distortion, the surface nodes contained in a *shadow area* (the portion of the duct surface defined by the projection of the tip of the thermowell) [27] had to follow the tip of the sensor during the morphing action. This task was accomplished assigning to the shadow area an appropriate rotation around the pipe axis and a translation in the direction of the axis itself (in two additional RBF solutions), in order to always keep it under the tip. The problem related to such corrective solutions is the absence of source points on the duct surface outside the shadow area that caused the loss of direct control on the morphing of the surface itself. This lack of control causes the distortion of the cylindrical duct surface visible in Fig. 5 (obtained with a 15° rotation of the shadow area, corresponding to the maximum expected shadow rotation during the unsteady FSI calculation).

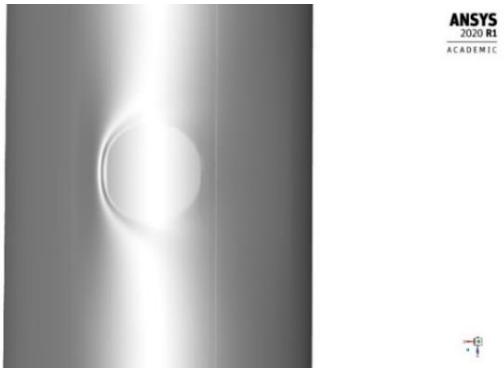

Fig. 5. Cylinder distortion

ICCS Camera Ready Version 2021
To cite this paper please use the final published version:
DOI: 10.1007/978-3-030-77977-1_37

To solve this issue a third RBF corrective solution derived from an STL-target solution was implemented. An STL-target motion type allowing to project the selected nodes onto a target surface (and therefore recovering the cylindricity of the duct) was assigned to the nodes belonging to the distorted portion of the cylinder (after the 15° rotation of the shadow). By tracking the position of the affected nodes in the three available meshes (the undeformed one, the distorted one after the maximum shadow rotation and the recovered one after the STL-target), it was possible to build a new RBF solution in which the source points were the nodes extracted from the starting duct surface mesh and their displacement was calculated as the difference between their corresponding position in the recovered mesh and in the distorted mesh.

By doing so it was possible to setup a recovery solution defined starting from the undeformed mesh and with an associated displacement able to recover the portion of the displacement imposed by the rotation of the shadow area that caused the distortion of the cylindrical surface. Therefore, if the rotation of the shadow area is applied with an amplification factor lower than the maximum one (i.e. 15°), the cylindricity of the duct can be recovered over-imposing this STL-target-derived solution with a proportional amplification factor.

Fig. 6 reports the volume mesh around the thermowell tip obtained after morphing applying the described correction procedure. Fig. 6 also shows the morphed surface mesh in the shadow region. The improvement in morphing quality, the correct positioning of the shadow area and the preservation of the cylindricity of the duct can be noticed.

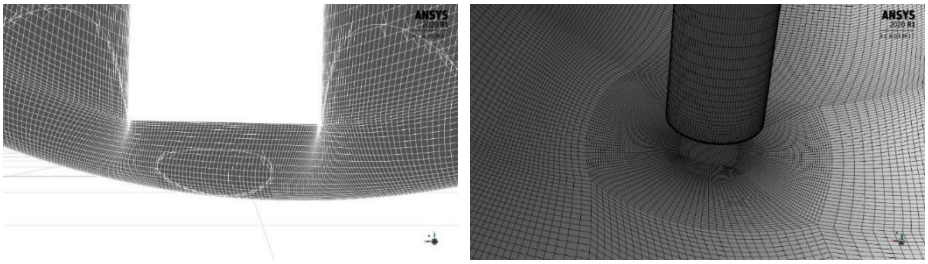

Fig. 6. Deformed mesh around the tip (left) and deformed surface mesh (right), with the corrective solutions

All the exposed RBF solutions were built using the bi-harmonic function, that allowed to achieve a high-quality morphing able to guarantee a low mesh distortion and the preservation of the boundary layers [28]:

$$\phi(r) = r \tag{13}$$

ICCS Camera Ready Version 2021
To cite this paper please use the final published version:
DOI: 10.1007/978-3-030-77977-1_37

4.3 CFD and FSI setups

The fluid dynamic domain was discretized by a structured and multiblock mesh composed of 3.16M hexahedrons. In order to solve the wall boundary layer up to the wall the thickness of the first layer of cells has been set to obtain a nondimensional wall distance y^+ lower than one. The adopted turbulence model was the SST k-ω. The velocity-inlet boundary condition was set to the inlet imposing a flow velocity equal to 6.4 m/s. A pressure-outlet condition was set at the outlet. Unsteady incompressible RANS calculation was run with a time-step set to 10^{-4} s. The structural damping ratio was set to 0.041, using the guidance found in literature [29]. The mesh is updated every time step computing the modal coordinates and the amplification factors of the corrective solutions.

4.4 Damping ratio

The value of the damping ratio of the system was not available for the experimental reference. As it is expected in the 0.01 to 0.07 range [29], a parametric study of its sensitivity with respect to the computed amplitude and the computed frequency has been carried out.

Table 1 reports the results of the sensitivity study. It can be clearly stated that a 0.041 damping ratio, inside the expected range, is able to reproduce the experimental results with sufficient accuracy. For this reason, such value was chosen.

Table 1. Results of the parametric study

Damping ratio	Maximum RMS transverse tip displacement at dynamic steady state [mm]	Relative error [%]
0.01	Not reached	-
0.02	Not reached	-
0.05	6.45	22.3
0.04	8.48	-2.17
0.041	8.304	-0.048

4.5 FSI analysis results

The simulation ran on a HPC dense node equipped with 256 GB of RAM and four Intel® Xeon® Gold 6152 CPUs, each of them featuring 22 cores @ 2.1 GHz. Out of the overall 88 cores, 30 were used to run the simulation until a dynamic constant periodic state was reached, after about 5 days of computation. Extrapolating the results obtained in previous studies [30, 31], the time needed to face the simulation with the same time-step size and simulated flow time by means of a full two-way coupling approach would have been approximately 60 days. The time needed to face the simulation of the rigid case with the same time-step size and simulated flow time is about 5 days.

In Fig. 7 and Fig. 8 the contours of the velocity magnitude on a plane perpendicular to the thermowell axis are displayed at two different flow-times corresponding to the maximum transverse displacements, both in the positive and in the negative direction.

ICCS Camera Ready Version 2021
To cite this paper please use the final published version:
DOI: 10.1007/978-3-030-77977-1_37

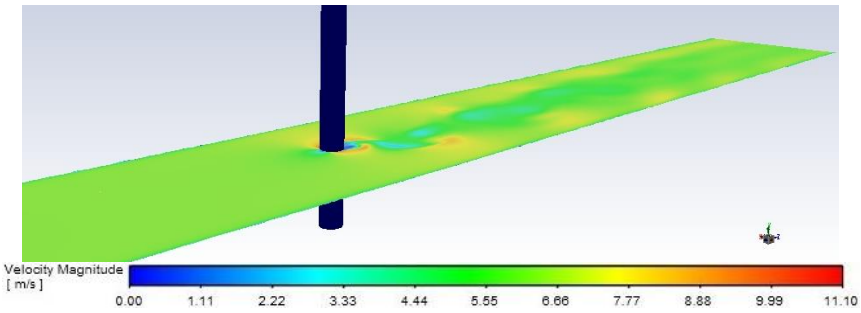

Fig. 7. Velocity magnitude contours at *t=0.8425 s*

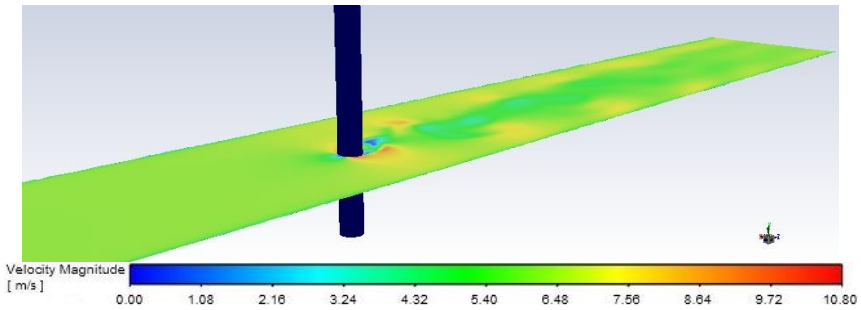

Fig. 8. Velocity magnitude contours at *t=0.8525 s*

In Fig. 9 the temporal evolution of the side force on the thermowell is displayed; Fig. 9 also depicts the temporal evolution of the transverse tip displacement. It can be observed that the maximum RMS transverse tip displacement is 8.304 mm, in good agreement with the available experimental data. The distributions of power spectral density of the two signals (the temporal evolution of the side force and of the transverse tip displacement) as a function of the frequency are shown in Fig. 10. For both signals a dominant frequency of 48.8 Hz was observed, confirming the correct capture of the lock-in condition.

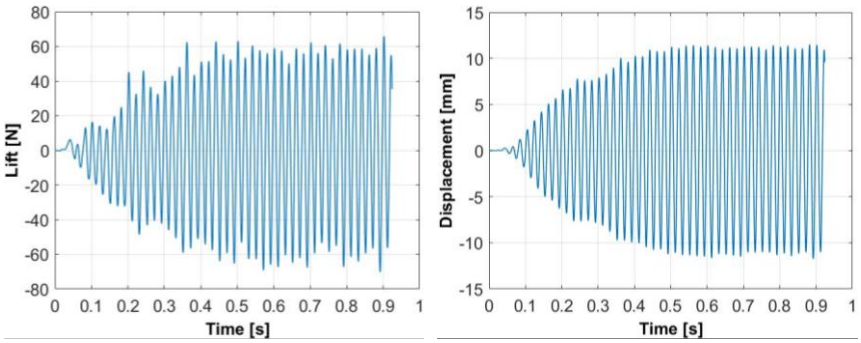

Fig. 9. Temporal evolution of the lift on the thermowell (left) and of the transverse tip displacement (right)

ICCS Camera Ready Version 2021
To cite this paper please use the final published version:
DOI: 10.1007/978-3-030-77977-1_37

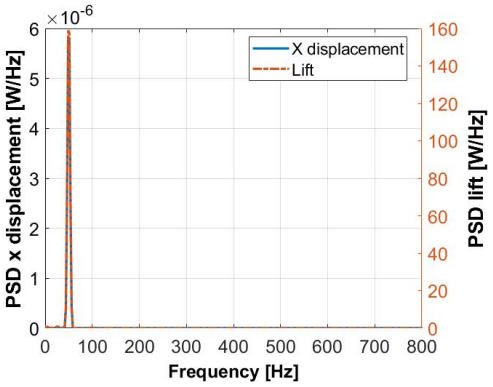

Fig. 10. Power spectral density distributions of the lift and of the transverse tip displacement

5 Conclusions

The presented work focused on an FSI analysis methodology based on the modal superposition approach. It was applied to the study of the vortex induced vibration of a thermowell. The problem of mesh adaptation was faced by an RBF based mesh morphing technique that allowed to provide a particular fast and robust configuration. The method consists in the extraction of a set of modal shapes, by a structural modal analysis, to be used for the implementation of a parametric mesh to be amplified according to modal coordinates computed during the progress of the CFD computation. The numerical configuration obtained is then an intrinsically aeroelastic fluid dynamic domain.

The studied configuration represents a particular challenging problem for the mesh morphing tool. The proximity of fixed and moving boundaries, in fact, involves strong distortion of the mesh which significantly limit the tolerable displacement. The adopted morphing software allowed to setup a particular efficient set of corrective solutions that made possible to manage very large displacement if compared to the dimension involved. The results of the implemented unsteady FSI analysis were compared to experimental data providing good agreement with measurements.

Further developments of this work might include gathering more comprehensive experimental data concerning the frequency of the thermowell vibration and the damping ratio of the system. The analysis could also be extended to other fluid velocity to capture the lock-in region of the in-line vibration and the lock-off regions. Other mesh setups, turbulence models and transition criteria could be investigated and compared to the results obtained with the current configuration.

References

1. Biancolini, M. E., Cella, U., Groth, C., and Genta, M.: Static Aeroelastic Analysis of an Aircraft Wind-Tunnel Model by Means of Modal RBF Mesh Updating. Journal of Aerospace Engineering **29**(6) (2016), https://doi.org/10.1061/(ASCE)AS.1943-5525.0000627

ICCS Camera Ready Version 2021
To cite this paper please use the final published version:
DOI: 10.1007/978-3-030-77977-1_37

2. Biancolini, M. E., Cella, U., Groth, C., Chiappa, A., Giorgetti, F., and Nicolosi, F.: Progresses in fluid-structure interaction and structural optimization numerical tools within the EU CS RIBES project. Computational Methods in Applied Sciences **49**, 529–544 (2019), https://doi.org/10.1007/978-3-319-89890-2_34
3. Di Domenico, N., Groth, C., Wade, A., Berg, T., and Biancolini, M. E.: Fluid structure interaction analysis: Vortex shedding induced vibrations. In Procedia Structural Integrity **8**, 422–432 (2018), https://doi.org/10.1016/j.prostr.2017.12.042
4. Groth, C., Cella, U., Costa, E., and Biancolini, M. E.: Fast high fidelity CFD/CSM fluid structure interaction using RBF mesh morphing and modal superposition method. Aircraft Engineering and Aerospace Technology **91**(6), 893–904 (2019), https://doi.org/10.1108/AEAT-09-2018-0246
5. RBF Morph: RBF Morph User's Guide. (2020)
6. Meirovitch, L.: Fundamentals of Vibrations. McGraw-Hill higher education, McGraw-Hill (2001)
7. Beckert, A., and Wendland, H.: Multivariate interpolation for fluid-structure-interaction problems using radial basis functions. Aerospace Science and Technology **5**(2), 125-134 (2001)
8. van Zuijlen, A. H., de Boer, A., and Bijl, H.: Higher-order time integration through smooth mesh deformation for 3D fluid–structure interaction simulations. Journal of Computational Physics **224**(1), 414-430 (2007)
9. Jin, R., Chen, W., and Simpson, T. W.: Comparative studies of metamodelling techniques under multiple modelling criteria. Structural and Multidisciplinary Optimization **23**(1), 1-13 (2001)
10. Biancolini, M. E., Costa, E., Cella, U., Groth, C., Veble, G., and Andrejašič, M.: Glider fuselage-wing junction optimization using CFD and RBF mesh morphing. Aircraft Engineering and Aerospace Technology, **88**(6), 740–752 (2016), https://doi.org/10.1108/AEAT-12-2014-0211
11. Papoutsis-Kiachagias, E. M., Andrejasic, M., Porziani, S., Groth, C., Erzen, D., Biancolini, M. E., … Giannakoglou, K. C.: Combining an RBF-based morpher with continuous adjoint for low-speed aeronautical optimization applications. In ECCOMAS Congress 2016 - Proceedings of the 7th European Congress on Computational Methods in Applied Sciences and Engineering **3** (2016)
12. Groth, C., Chiappa, A., Biancolini, M. E.: Shape optimization using structural adjoint and RBF mesh morphing. Procedia Structural Integrity **8**, 379–389 (2018), https://doi.org/10.1016/j.prostr.2017.12.038
13. Papoutsis-Kiachagias, E. M., Porziani, S., Groth, C., Biancolini, M. E., Costa, E., and Giannakoglou, K. C.: Aerodynamic Optimization of Car Shapes Using the Continuous Adjoint Method and an RBF Morpher. Computational Methods in Applied Sciences **48**, 173–187 (2019), https://doi.org/10.1007/978-3-319-89988-6_11
14. Porziani, S., Groth, C., Waldman, W., and Biancolini, M. E.: Automatic shape optimisation of structural parts driven by BGM and RBF mesh morphing. International Journal of Mechanical Sciences, 189, 105976 (2021)
15. Biancolini, M. E., Chiappa, A., Giorgetti, F., Groth, C., Cella, U., and Salvini, P.: A balanced load mapping method based on radial basis functions and fuzzy sets. International Journal for Numerical Methods in Engineering **115**(12), 1411–1429 (2018), https://doi.org/10.1002/nme.5850
16. Groth, C., Costa, E., and Biancolini, M. E.: RBF-based mesh morphing approach to perform icing simulations in the aviation sector. Aircraft Engineering and Aerospace Technology **91**(4), 620–633 (2019), https://doi.org/10.1108/AEAT-07-2018-0178

ICCS Camera Ready Version 2021
To cite this paper please use the final published version:
DOI: 10.1007/978-3-030-77977-1_37

17. Giorgetti, F., Cenni, R., Chiappa, A., Cova, M., Groth, C., Pompa, E., and Biancolini, M. E.: Crack Propagation Analysis of Near-Surface Defects with Radial Basis Functions Mesh Morphing. In Procedia Structural Integrity **12**, 471–478 (2018), https://doi.org/10.1016/j.prostr.2018.11.071
18. Pompa, E., D'Amico, G., Porziani, S., Giorgetti, F., Groth, C., Portone, A., Biancolini, M. E.: Crack propagation analysis of ITER Vacuum Vessel port stub with Radial Basis Functions mesh morphing. Fusion Engineering and Design **157**, 111617 (2020)
19. Groth, C., Porziani, S., Chiappa, A., Pompa, E., Cenni, R., Cova, M., ..., Rochette, M.: High fidelity numerical fracture mechanics assisted by RBF mesh morphing. Procedia Structural Integrity **25**, 136-148 (2020)
20. Chiappa, A., Groth, C., Biancolini, M. E.: Improvement of 2D finite element analysis stress results by radial basis functions and balance equations. International Journal of Mechanics **13**, 90-99 (2019)
21. Chiappa, A., Groth, C., Brutti, C., Salvini, P., Biancolini, M. E.: Post-processing of 2D FEM Q1 models for fracture mechanics by radial basis functions and balance equations. International Journal of Mechanics **13**, 104-113 (2019)
22. Chiappa, A., Groth, C., Reali, A., Biancolini, M. E.: A stress recovery procedure for laminated composite plates based on strong-form equilibrium enforced via the RBF Kansa method. Composite Structures, 112292 (2020)
23. Biancolini, Marco E.: Mesh morphing and smoothing by means of Radial Basis Functions (RBF): a practical example using fluent and RBF morph. Handbook of Research on Computational Science and Engineering: Theory and Practice, IGI Global, Hershey, PA (2012)
24. Emerson: https://www.emerson.com/en-us/asset-detail/rosemount-twisted-square-a-new-twist-on-thermowell-design-1800740 (2017)
25. Boyer, H. E., Gall, T. L.: Metals Handbook. Eds., American Society for Metals, Materials Park, OH (1985)
26. RBF Morph: RBF Morph – Modelling Guidelines and Best Practices Guide. (2020)
27. Costa, E., Biancolini, M. E., Groth, C., Caridi, D., Lavedrine, J., Dupain, G.: Unsteady FSI analysis of a square array of tubes in water crossflow. Flexible Engineering Toward Green Aircraft, Springer (2020)
28. Biancolini, M. E., Chiappa, A., Cella, U., Costa, E., Groth, C., Porziani, S.: Radial Basis Functions Mesh Morphing - A Comparison Between the Bi-harmonic Spline and the Wendland C2 Radial Function. International Conference on Computational Science, 294-308 (2020), https://doi.org/10.1007/978-3-030-50433-5_23
29. Adams, V., Askenazi, A.: Building Better Products with Finite Element Analysis. OnWord Press, Santa Fe, N. M. (1999)
30. Geronzi, L., Gasparotti, E., Capellini, K., Cella, U., Groth, C., Porziani, S., Chiappa, A., Celi, S., Biancolini, M. E.: Advanced Radial Basis Functions mesh morphing for high fidelity Fluid-Structure Interaction with known movement of the walls: simulation of an aortic valve. International Conference on Computational Science, 280-293 (2020), https://doi.org/10.1007/978-3-030-50433-5_22
31. Geronzi, L., Gasparotti, E., Capellini, K., Cella, U., Groth, C., Porziani, S., Chiappa, A., Celi, S., Biancolini, M. E.: High fidelity fluid-structure interaction by radial basis functions mesh adaption of moving walls: A workflow applied to an aortic valve. Journal of Computational Science **51**, 101327 (2021), https://doi.org/10.1016/j.jocs.2021.101327

ICCS Camera Ready Version 2021
To cite this paper please use the final published version:
DOI: 10.1007/978-3-030-77977-1_37